Geosystems and Geoenvironment 1 (2022) 100036

Contents lists available at ScienceDirect

Geosystems and Geoenvironment

journal homepage: www.elsevier.com/locate/geogeo

Evidence that the GOE was a prolonged event with a peak around 1900 Ma

Ross R. Large[a,*], Robert M. Hazen[b], Shaunna M. Morrison[b], Dan D Gregory[c], Jeffrey A. Steadman[a], Indrani Mukherjee[a]

[a] Earth Science CODES, University of Tasmania, 7005 Australia
[b] Earth & Planets Laboratory, Carnegie Institution for Science, Washington DC 20015, United States of America
[c] Geology Dept., University of Toronto, Ontario, Canada

ARTICLE INFO

Article history:
Received 16 January 2022
Revised 31 January 2022
Accepted 7 February 2022

Keywords:
Pyrite proxy
Great oxygenation event
Paleoproterozoic
Archean
Atmospheric oxygen
Deep time

ABSTRACT

The great oxygenation event (GOE), the first of two major rises in atmospheric oxygen in Earth history, was initially placed near the Archean-Proterozoic boundary (~2500 Ma). More recently, the position of the GOE has been moved to between 2500 and 2300 Ma so as to coincide with the loss of the MIF sulfur isotope signal due to the creation of the Earth's ozone layer at that time. Here we present a revised interpretation of the history of atmospheric oxygen in the Archean and Proterozoic, based on a multi-geochemical proxy approach. Integration of a large database of analyses of redox sensitive elements in sedimentary pyrite (Se, Co, Mo), the matrix of black shales (U, Mo), and the temporal evolution of redox sensitive minerals, suggest Earth's first oxygenation was prolonged, reaching a peak between 2000 and 1700 Ma. Rather than a relatively short-lived event from 2500 to 2300 Ma, we suggest an alternative profile for Earth's atmospheric O_2, i.e., an unsteady start to the rise in oxygen around 2700 Ma that undulated for approximately a billion years, reaching a peak around 1900 Ma before a plunge in the Proterozoic Eon after 1700 Ma.

1. Introduction

A major increase in oxygen (the GOE) was first suggested (Cloud, 1972; Holland, 1984) by the global occurrence of thick successions of banded iron formations toward the end of the Archean Eon. Although this theory has been rejected by most in favor of iron precipitation by anoxygenic phototrophic Fe-oxidizing organisms (Kappler et al., 2005), the build-up of Fe^{2+} in the oceans required to form banded iron formation is an indicator of low oxygen levels in the Archean. As prokaryotic life began to flourish in the Neoarchean oceans, excess oxygen remaining after reduction by $Fe^{2+}$and organic matter eventually was liberated to the atmosphere, initially causing surface oxidation and then accumulating to produce the GOE (Cloud, 1972). A more precise control on the timing of the GOE was developed following the recognition of mass-independent fractionation of S-isotopes (MIF-S) in Archean sedimentary pyrite (Farquhar et al., 2000), which suggested that the absence of MIF signals in sedimentary rocks between 2500 and 2300 Ma was related to the first appearance of the ozone layer (Farquhar and Wing, 2003; Farquhar et al., 2011). On the other hand, many studies have reported evidence for mild to strong oxygenation of the Archean atmosphere and upper oceans prior to the GOE (Towe, 1990; Anbar et al., 2007; Ohmoto et al., 2006; Lyons et al., 2014). Notwithstanding these many studies, the prevailing consensus remains that a significant ($>10^{-3}$ present atmospheric level, or "PAL") and sustained rise in the global atmospheric oxygen did not take place before 2500 Ma and occurred over a time frame of less than 200 million years (Lyons et al., 2014).

Here we address the issues of the timing, duration, and peak of the GOE by applying recent studies on two relatively new proxies, (1) the redox-sensitive trace element chemistry of sedimentary pyrite and black shale matrices, and (2) the redox evolution of crustal minerals. We compare our results with some previously proposed ocean/atmosphere proxies and suggest an alternative profile for the GOE.

2. Analytical methods

The U and Mo composition of the fine matrix portion of the shales were measured in situ by laser ablation-inductively coupled

* Corresponding author.
E-mail address: Ross.large@utas.edu.au (R.R. Large).

https://doi.org/10.1016/j.geogeo.2022.100036

Table 1
Summary of pyritic black shale details used to determine Se/Co ratios in pyrite plotted in Fig. 2A.

Eon	Number of Formations	Number of black shale samples	Number of pyrite analyses	Geographic coverage
Archean (3550–2500 Ma)	14	52	719	Australia, South Africa, Canada
Paleoproterozoic (2500–1600 Ma)	12	64	349	Canada, Australia, Russia, Finland, India
Mesoproterozoic (1600–1000 Ma)	6	29	263	Russia, Australia, India
Neoproterozoic (1000- 540 Ma)	17	45	453	China, Australia, Zambia, USA

plasma mass spectrometry (LA-ICPMS) at the centre for Ore Deposits and Earth Science, University of Tasmania. Eight to ten spots were measured per sample on areas with the lowest pyrite and detrital phases and averaged to obtain the final result. The measurements were done using a 193 nm ArF Excimer ATL Atlex ILR laser coupled to an Agilent 7700 ICP mass spectrometer. The system is equipped with a custom-made constant-geometry Laurin Technic ablation chamber S-155 designed for 20 mounts of 2 cm size. A 50 μm spot was analysed using a laser pulse rate of 10 Hz and a laser beam fluence ~2 J/cm^2 at the sample. Sedimentary pyrite analyses were carried out in the same laboratory with the same equipment, to obtain Se, Co, and Mo content of sedimentary pyrite. Details on the selection of pyrite for analysis and the LA-ICPMS method and standards used for analysis are reported in detail elsewhere (Large et al., 2014, 2017, 2018).

The data measurements for Se/Co and Mo in sedimentary pyrite are from 171 samples involving 1535 spot analyses of pyrite. The data measurements for Mo and U in shale matrix are from the analysis of 82 black shale samples, involving 1275 LA-ICPMS analyses. The samples are principally from deep drill cores from below the level of surface oxidation and have been studied petrographically to ensure they are not affected by later alteration or significant metamorphism. The full analytical data used to generate the Se/Co proxy trend in Fig. 2a have been previously published in Large et al. (2014, 2017, 2018) and Steadman (2020) and are not repeated here. Details of the samples analysed in the Precambrian dataset are given in Steadman et al. (2020) and further summarised in Table 1.

3. Trace element chemistry of sedimentary pyrite

Temporal trends in redox-sensitive elements (RSE) in black shales have been used as proxies for ocean-atmosphere oxygenation for over 30 years (Holland, 1984). Molybdenum, Se, U, V, Ni, Tl, Cr, and *Re* are some of the elements or their isotopes used as oxygenation proxies. The main principle behind their use is that an increase in atmosphere oxygen causes continental oxidation and erosion of pyrite, which leads to the release of RSE into the river systems and ultimately the ocean. Most of the RSE are nutrient elements taken up by marine organisms to be eventually deposited in seafloor black shales formed in anoxic to euxinic environments. Significant increases in RSE in ancient black shales are thus taken as an indication of increased atmosphere oxygenation. However, there are a number of limitations in this approach, including the capacity to eliminate the effects of weathering, diagenesis, and metamorphism on RSE concentration in black shales, the effects of detrital components on the RSE concentration, and partitioning of RSE between different minerals in the rock, under differing paleoredox conditions on the seafloor (Large et al., 2014; Planavsky et al., 2020). In order to overcome these limitations, the sedimentary pyrite proxy was developed (Large et al., 2014).

This proxy is based on the same principle, except the RSE are measured in sedimentary pyrite by laser ablation inductively coupled mass spectrometry (LA-ICPMS) rather than the bulk rock method. Measurements can be performed within a single pyrite grain domain, avoiding the problem of temporal variation in the composition of shales, due to the in situ nature of the analytical technique. Most importantly, petrographic textural analyses of pyrite allow detection of effects of diagenesis, metamorphism, alteration, and hydrothermal activity, all of which affect trace element concentrations (Large et al., 2014; Planavsky et al., 2020).

3.1. Se/Co in pyrite

Selenium and cobalt are both RSE and tightly held in the pyrite structure, however they are redox opposites in the sense that Se becomes more soluble with a long residence time, and therefore more abundant in seafloor pyrite under increasing ocean-atmosphere oxygenation, whereas Co becomes less soluble with a short ocean residence time and less abundant in sedimentary pyrite (Steadman et al., 2020). The ratio Se/Co in sedimentary pyrite has thus been shown to be extremely sensitive to changes in atmospheric oxygenation, varying over five orders of magnitude from low atmosphere oxygen (<0.2 PAL) to high atmosphere oxygen (1 to 1.5 PAL; Fig. 1). Our results from the LA-ICPMS analyses of 1482 sedimentary pyrites for black shales from 3550 to 800 Ma (Fig. 2a) show that the median Se/Co ratio exhibits low values (<0.05) through the Paleo- and Mesoarchean, rising to a peak of ~0.1 in the Neoarchean, then rising again to a maximum in the Paleoproterozoic of around 1 to 10 between 2000 and 1800 Ma (predicted to be 15 to 25 wt% O_2; Steadman et al., 2020), before falling back to between 0.1 and 0.05 in the Meso- and Neoproterozoic. The currently accepted position of the GOE around 2500–2300 Ma is within the period when Se/Co rises from 0.1 to 1. The robust character of the two peak periods of Se/Co from 2800 to 2500 Ma and 2000 to 1700 Ma is indicated by their representation by samples from diverse geographic locations and global sedimentary basins (Steadman et al., 2020; Table 1).

4. Uranium and molybdenum concentration in black shale matrix

The same samples analysed for Se, Co, and Mo in pyrite were analysed for U and Mo in the black shale organic-clay matrix. Previous studies on Mo and U in bulk rock black shales demonstrated the immense value of these RSE as oxygenation proxies (Scott et al., 2008). Most previous research on the RSE Mo and U in sedimentary rocks has employed bulk rock analyses, which measure both the detrital and authigenic components (Scott et al., 2008). Here we are interested only in the authigenic component and developed the technique of laser ablation ICPMS analyses of both the sedimentary pyrite (for Mo, Se, and Co) and the fine carbonaceous-clay matrix (for U, Mo, and REE) that avoids the coarse-grained detrital components that may also be a source of these elements in black shales (Large et al., 2018). Our data (Fig. 2c, d) show a general increase in the two RSE through the Neoarchean, with Mo reaching a maximum in the Paleoproterozoic from 1800 to 1600 Ma, whereas U reaches a maximum from 2000 to 1600 Ma.

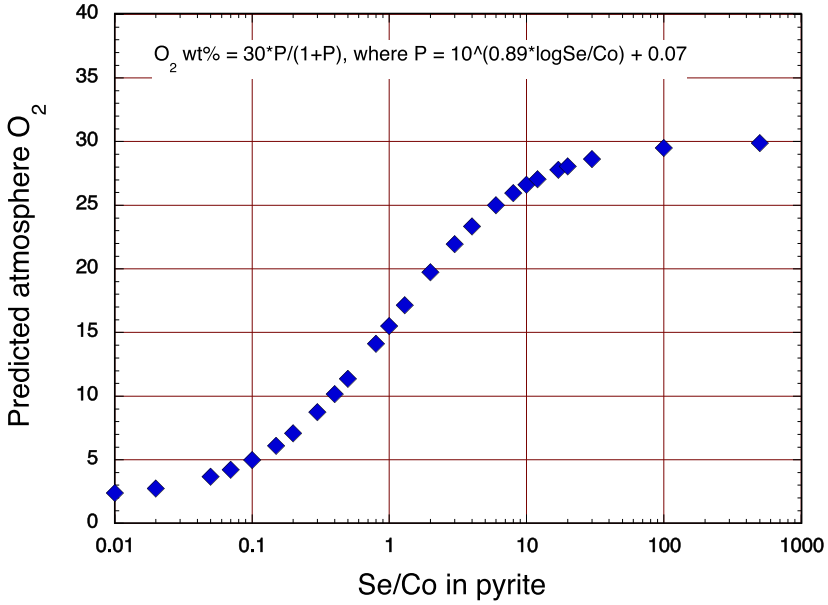

Fig. 1. Relationship between Se/Co ratio in sedimentary pyrite and estimated oxygen concentration in the atmosphere in wt% O_2 (Steadman et al., 2020).

5. Mineral evolution in the precambrian

The past decade has seen a significant effort to collate and analyze data on the ages, distributions, and nature of minerals through deep time (Hazen et al., 2008). More than 200,000 mineral species/locality/age records, coupled with information on mineral properties (notably, composition and oxidation states), coexisting species, geological and tectonic contexts, dating techniques, age uncertainties, and links to primary sources, are now collated in the open-access Mineral Evolution Database Golden (2019; MED: https://rruff.info/ evolution). Investigations of the appearance of new minerals over the past 3.5 billion years, in some instances accompanied by their redox states, reveal a striking pattern of episodic mineralization, which correlates with significantly enhanced mineral production and preservation during five presumed periods of supercontinent assembly (Hazen et al., 2008).

Data in the MED document a modest shift in mineral chemistry during the interval from ~2700 to 1500 Ma. Prior to this period, most minerals were silicates, sulphides, and carbonates, with volumetrically less significant occurrences of oxides, arsenides, sulfosalts, and other phases. Changes are also observed in the distribution of oxide/hydroxide minerals. Starting at ~2700 Ma, transition metal mineral species, particularly magnetite and Fe^{3+} phases, occurred in BIFs, while oxides/hydroxides of Mn, Cu, Co, V, and other redox-sensitive elements became more abundant. Note that a significant number of redox-sensitive minerals, including major deposits bearing hematite and Fe^{3+} oxide/hydroxides and a host of new oxidised secondary Co, Cr, Cu, Mn, V, and U minerals, appear after ~2000 Ma. This trend in the introduction of new oxidised minerals, coupled with the observed gradual increase in average redox state of transition elements, demonstrates that mineral occurrence data serves as a useful proxy for Earth's oxygenation (Hummer et al., 2020; Golden et al., 2013).

The temporal pattern of mineral evolution (Fig. 2b) shows a definite similarity to the Se/Co pyrite proxy with a secondary peak from 2800 to 2500 Ma and the major peak in mineral evolution from 2000 to 1700 Ma. A calculation of the relative redox of mineral species (color of bars in Fig 2b) shows a gradual increase in their oxidation state from 3000 to 1600 Ma.

6. Discussion

The coincidence of the major peak in the Se/Co pyrite proxy with the major peak in mineral evolution around 2000 to 1700 Ma is striking (Fig. 2a, b) and is the basis of our hypothesis that atmosphere oxygen was at a maximum over this time interval, rather than the accepted position of the GOE, 300 to 500 million years earlier. The trends and maxima of the two RSE Mo and U in the matrices of black shales provide some support, although not as definitive, both RSE peak between 2000 and 1600 Ma. The secondary peak in mineral evolution at 2800 to 2500 Ma is also matched by a less well-developed maximum in the Se/Co pyrite proxy, but is not obvious from the Mo and U data. These four proxies generally decrease from 1600 to 1000 Ma suggesting that the ocean-atmosphere system suffered a consistent decline in oxygenation over this time period, with a possible spike around 1400 Ma (Mukherjee and Large, 2016).

Some researchers have proposed that the rise in oxygen before 2500 Ma might have been generated in local environments and not represent global oxygenation of the atmosphere-hydrosphere system (Anbar et al., 2007; Ostrander et al., 2021; Meixnerova et al., 2021). Lalonde and Konhauser (2015) suggest that local oxygen production and immediate consumption in surface-bound (benthic) microbial ecosystems at profound disequilibrium conditions may explain oxygen rises before 2500 Ma. In this same vein, the pyrite Se/Co proxy and mineral evolution burst around 2700 to 2500 Ma might indicate local rather than global signals for oxygenation, or otherwise, intermittent or transient oxygenation pulses.

6.1. Comparison with seven other atmosphere oxygen proxies

6.1.1. Marine evaporites

Marine evaporite sequences provide a record of elevated sea water sulfate and chloride contents, which are indicative of shallow water environments with increased atmosphere pO_2 and sea water salinity. The source of seawater sulfate is considered to be from a combination of oxidative erosion of continental pyrite and S-outgassing of volcanic magmas (Catling and Kasting, 2017), thus the lack of oxygen in the Archean Eon may have led to lower levels of sulfate in Archean oceans compared with the subsequent eons.

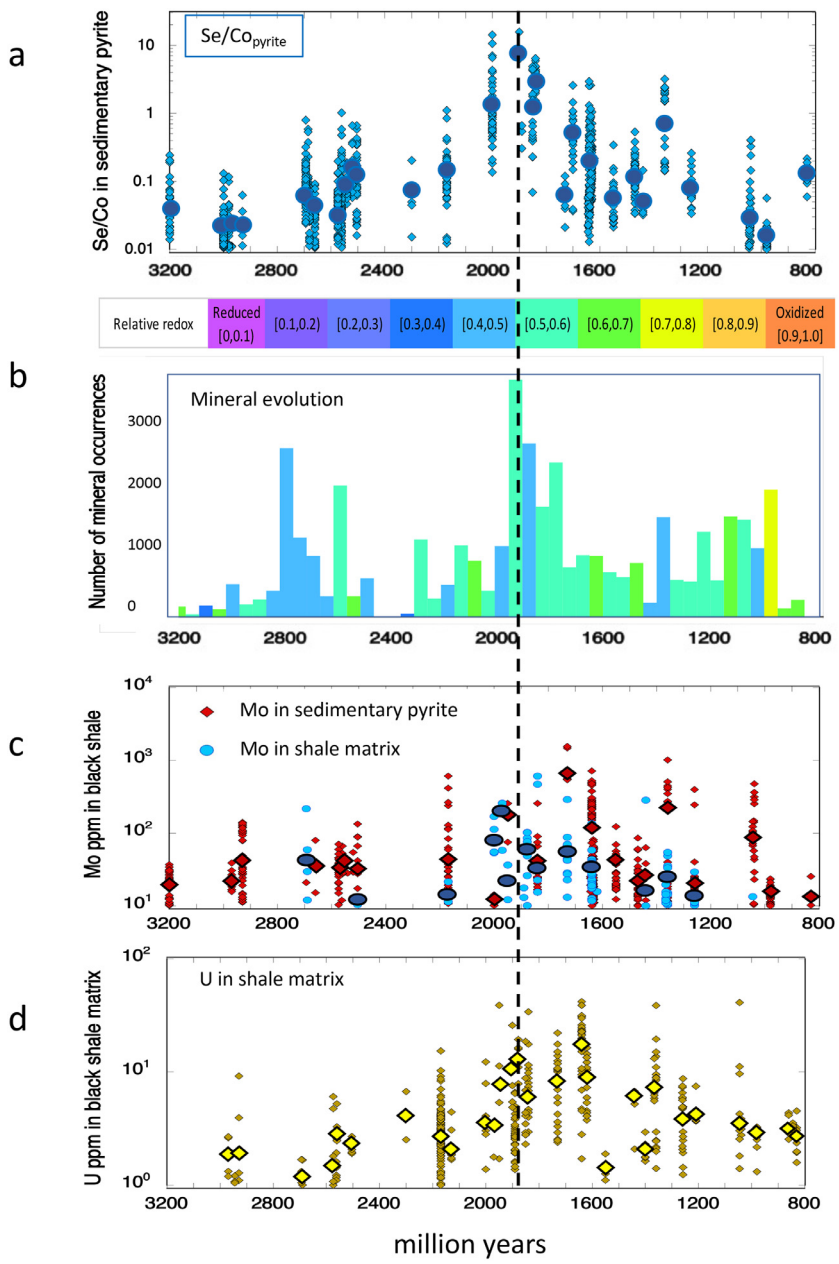

Fig. 2. Temporal variation between 3200 and 800 Ma based on data collected in this study. a) Se/Co ratio in sedimentary pyrite determined by LA-ICPMS; b) occurrence of mineral species, color of bars indicate the level of mean mineral cation oxidation; c) Mo content of both sedimentary pyrite and black shale matrix determined by LA-ICPMS; and d) U content of black shale matrix determined by LA-ICPMS.

Although Precambrian evaporites are far less abundant than those in the Phanerozoic Eon, Evans (2006) recorded over 100 Precambrian evaporite sequences, of which at least 10 are in the Archean.

The temporal distribution of the 27 most significant evaporite occurrences in the Precambrian are shown in Fig. 3, where they are compared with the number of reported occurrences of the four major minerals in evaporites; anhydrite, halite, sylvite, and magnesite (all data derived from the mineral evolution database). These patterns all show three dominant periods of evaporite formation at 2800–2400 Ma, 1900–1600 Ma and 1000–500 Ma; the first two corresponding with the proposed peaks in atmospheric oxygen suggested by the sedimentary pyrite proxy and general mineral evolution (Fig. 2).

6.1.2. Molybdenum isotopes

Molybdenum isotopes in black shales and carbonates have become recognised as a robust method of tracking ocean-atmosphere oxygenation (Wille et al., 2007; Thoby et al., 2019), although fewer measurements have been published compared to the proxies already discussed. Elevated $\delta^{98/95}$Mo above 0.7 is indicative of ocean-atmosphere oxygenation. Values of up to 2.0 are reported from shales, BIF, and carbonates in the interval 2800 to 2400 Ma, compared with a maximum of ~1.0 prior to 2800 Ma (Fig. 4c).

6.1.3. Sulfur isotopes

Discovery of the MIF-S signal in sedimentary pyrite was a major scientific breakthrough (Farquhar et al., 2000), and its interpretation as a precise marker of the GOE has become well accepted (Lyons et al., 2014; Pavlov and Kasting, 2002). However, the extended period of positive MIF-S between 2750 and 2450 Ma, during which Δ^{33}S commonly exceeds 6‰ (Fig. 4d), coincides precisely with the period of maximum Mo isotope values (Fig. 4c), the first pulse of mineral evolution (Fig. 4b), and increased sulfate evaporite mineral formation (Fig. 3). Whereas the strong positive

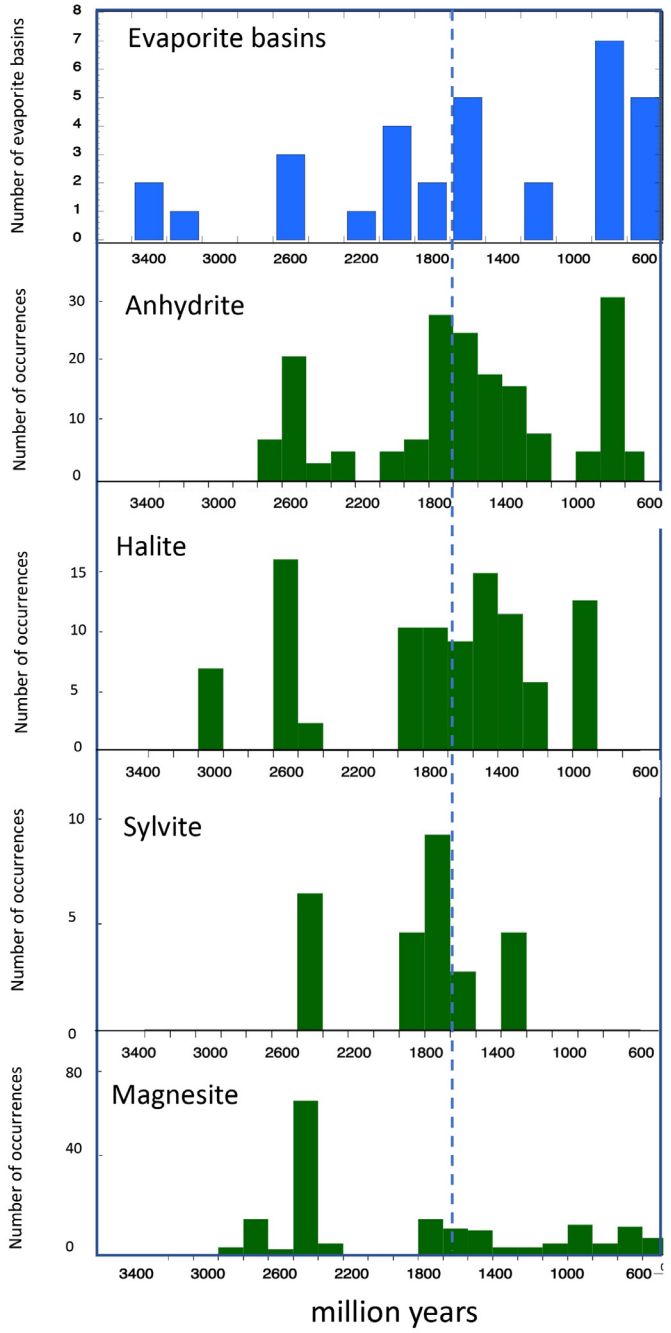

Fig. 3. Temporal distribution of major evaporite deposits from 2600 to 800 Ma compiled from Evans (2008), and temporal distribution of major evaporite mineral occurrences (Golden, 2019) anhydrite, halite, sylvite, and magnesite.

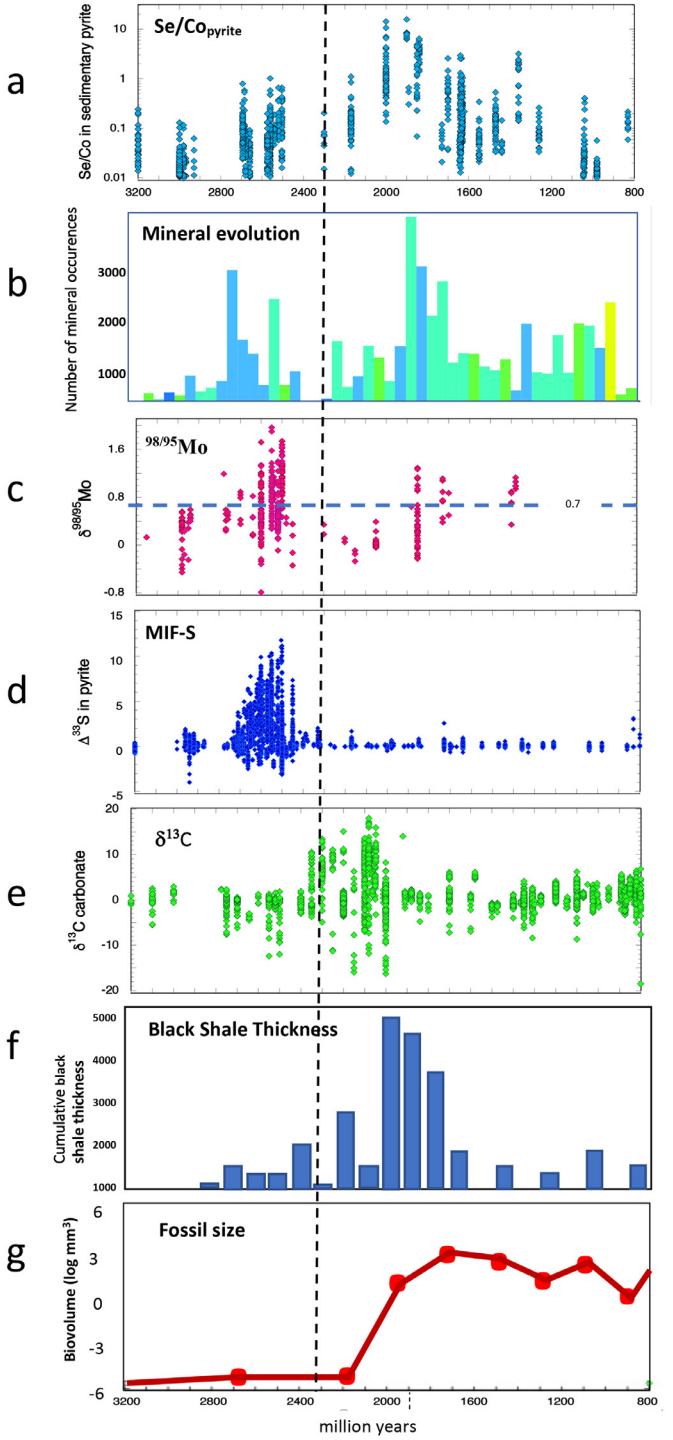

Fig. 4. Comparison of the temporal variation of various atmosphere-ocean oxygenation proxies: a) Se/Co in sedimentary pyrite (this study); b) occurrence of mineral species (this study); c) $\delta^{98/95}$Mo in marine sedimentary rocks (Wille et al., 2007; Thoby et al., 2019); d) MIF-S signal in sedimentary pyrite (Large et al., 2021; Killingsworth et al., 2019); e) δ^{13}C in marine carbonates (Shields and Veizer, 2002); f), h) cumulative black shale thickness (Condie et al., 2001); and i) maximum fossil size (Payne et al., 2009).

MIF-S signal is interpreted as indicating atmosphere oxygen was less than 10^{-5} PAL (Pavlov and Kasting, 2002; <2 ppm O_2), the other proxies indicate weakly oxygenated oceans at the same time when cyanobacteria and increased ocean sulfate were developing.

The end of the MIF-S signal (Fig. 4d), which takes place over the period 2450 to 2300 Ma, is interpreted as an expression of the GOE. However in contrast, this event corresponds to a drop in seawater Mo-isotopes to near zero (Fig. 4c), together with a rise in δ^{13}C in sedimentary carbonates known as the Lomagundi excursion (Melezhik et al., 2007; Fig. 4e) and a period of about 200 million years (2400 to 2200 Ma), which saw no new minerals appear in the rock record (Fig. 4b). Farquhar and Wing (2003) recognised that MIF-S did not completely disappear around 2400 Ma, but continued with a much reduced signal from 2450 Ma to approximately 2000 Ma: their Stage II. This period (2450 to 2000 Ma) is interpreted to record either the onset of oxidative weathering or stabilization of atmospheric oxygen and ozone to intermediate levels, that would still allow photolysis of SO_2 and SO. If the second hypothesis is correct, then it fits well with our suggestion, that the GOE was a protracted event that extended up to, and even be-

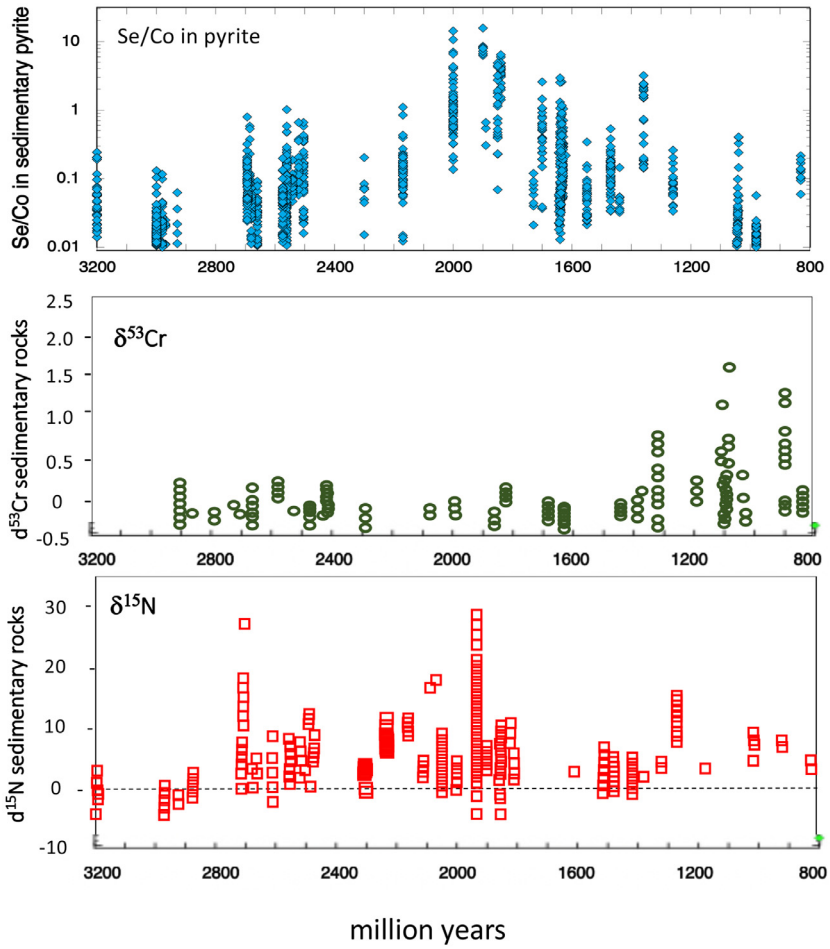

Fig. 5. Comparison of temporal pattern of Se/Co ratio in sedimentary pyrite in black shales with δ^{53}Cr for sedimentary rocks (Cole et al., 2016; carbonates, iron formations/ironstones and black shales), and δ^{15}N for sedimentary rocks (Stueken et al., 2016; Cheng et al., 2019).

yond, ca. 2000 Ma, when MIF-S finally and completely disappeared due to the development of a full-blown ozone layer (Farquhar and Wing, 2003). In further support, recent micro-beam S-isotope analyses on pyrite by Philppot et al. (2018) demonstrate an intermittent MIF-S signal between 2450 and 2310 Ma which they also suggest requires re-evaluation of the position of the GOE.

6.1.4. Thickness of black shales

There is agreement that the Lomagundi C-isotope excursion (Fig. 4e) represents a long period of burial of organic carbon from 2350 to 1950 Ma, which would have resulted in a large-scale release of oxygen to the atmosphere (Melezhik et al., 2007; Lyons et al., 2014). Changes in thickness of Precambrian black shales over time, which can be used as a rough proxy for atmospheric oxygen, provides support for this concept. A compilation of global black shale thickness by Condie et al. (2001; Fig. 4f) indicates that significant black shale deposition started around 2700Ma increasing to the maximum Precambrian cumulative thickness from 2000 to 1900 Ma, followed by elevated thicknesses to 1700 Ma, supporting other evidence (Fig. 4) for maximum elevation in atmospheric oxygen.

6.1.5. Chromium isotopes

Chromium isotopes in sedimentary rocks have become a popular tool for tracking variations in the ancient ocean/atmosphere system. Chromium is a RSE and its isotopes are fractionated during redox reactions. Chromium on the continents is dominated by the less mobile Cr (III), whereas Cr in the marine environment is dominantly the more mobile Cr (VI). modeling suggests that during oxidative weathering, Cr (III) is converted to the more soluble Cr(VI) via Mn oxides, which are only stable in a relatively oxygenated environment. The level of isotope fractionation is taken as a proxy for oxygenation. Initial studies on Precambrian iron formations (Frei et al., 2009) indicated marginally elevated values above the crustal mean, possibly indicating mild oxygenation from 3000 to 2500 Ma and around 1900 Ma, but lower values during the period of the GOE from 2500 to 2300 Ma and from 1700 to 1400 Ma. A study of Cr isotopes in sedimentary ironstones from six locations through the Archean to Mesoproterozoic (Planavsky et al., 2014) showed little fractionation from the crustal value and was interpreted to suggest that atmosphere oxygen was less than 0.1% of PAL for the whole period. Follow-up research on black shales (Cole et al., 2016) again showed no significant fractionation over this period and importantly failed to show any fractionation in the interval of the GOE (Fig. 5b). More recent work (Fang et al., 2020) emphasises that a key point of the previous Cr isotope modeling is the generation of Cr (VI) in oxidative weathering during atmospheric oxygenation events. However, no direct evidence of Cr (VI) has yet been reported in sedimentary rocks. These authors (Fang et al., 2020) conclude that the application of Cr isotopes to atmosphere oxygenation in the Precambrian is limited for the present until a clear understanding of the global mass balance of Cr isotopes is achieved.

6.1.6. Nitrogen isotopes

Nitrogen isotope studies of bulk sedimentary rocks are being increasingly used to track ocean and atmosphere oxygenation

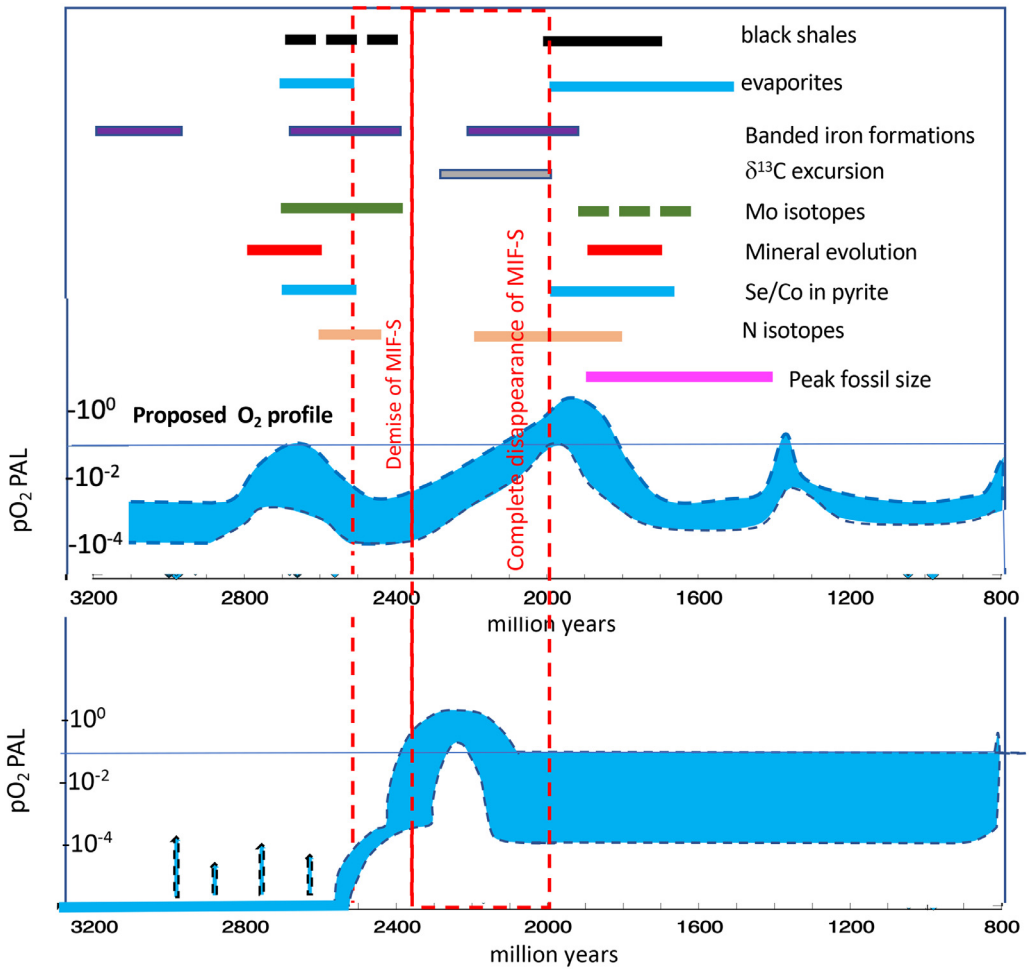

Fig. 6. Atmosphere oxygen proxy peak periods discussed in the text compared with the proposed new profile of the GOE (middle panel) and the generally accepted profile (Lyons et al., 2014; lower panel). The proxy periods in the upper panel are taken from the datasets in Figs. 1-5.

(Stueken et al., 2016; Cheng et al., 2019; Ossa et al., 2019). The marine N biogeochemical cycle is extremely complex and is affected by a large number of factors. However, considering N in the Precambrian in general terms, under very low oxygen conditions N isotope values ($\delta^{15}N$) are around −5 to +5 ‰, being possibly controlled by Mo-based biological N_2-fixation. Moderate levels of oxygenation are thought to stimulate an aerobic nitrogen cycle with N isotope values from +5 to +15 ‰ related to fixed-N losses, whereas high levels of ocean oxygenation will lead to a well-developed aerobic nitrogen cycle with fractionation controlled by partial denitrification and N-isotope values up to +30‰ and beyond. The compilation of N isotope data (Fig. 5c) may be interpreted to indicate very low ocean oxygenation from 3200 to 2800 Ma, followed by a rise from 2800 to 2500 Ma, dropping to a low at 2300 Ma, and then increasing to peak levels around 2000 to 1900 Ma. This pattern is similar to the Se/Co in pyrite proxy and the mineral evolution data, however it must be emphasised that the peaks in N isotope values are supported by data from only one sedimentary basin each at around 2700 and 1900 Ma.

6.1.7. Maximum size of organisms

In addition to evidence from the geochemical and geological proxies, at least one biological proxy also is consistent with our suggested profile of the GOE. The maximum size of organisms in the Precambrian increased enormously in the middle of the Palaeoproterozoic between 2000 and 1800 Ma (Payne et al., 2009; Fig. 4g). The macrofossil *Grypania spiralis* is a key example of this sudden increase in size (Payne et al., 2009). The curve of maximum body volume (Fig. 4g) peaks around 1800 Ma followed by a decline in known maximum organism size from 1600 to 900 Ma, matching the decline in Se/Co ratio of sedimentary pyrite and several other proxies that we interpret as indicating a decline in atmospheric oxygen over this period (Steadman et al., 2020; Figs. 2 and 4).

7. Significance

When most available geochemical proxies for ocean/atmosphere oxygenation are compared (Figs. 2, 4 and 5), the data suggest there were two periods of elevated atmospheric oxygen: one in the Neoarchean and the other in the Paleoproterozoic (Fig. 6). The first occurred around 2700 to 2400 Ma (peaking at ~2500 Ma) and the second from 2100 to 1700 Ma (peaking at ~1800 Ma), correlating with the amalgamation of the supercontinents Kenorland and Nuna respectively (Hazen et al., 2008). Supporting geological evidence includes the size of organisms, accumulated thickness of black shales and occurrence of evaporites, red-beds, Mn-deposits, and sedimentary copper deposits during these periods. A possible earlier period of oxygenation between 3500 and 3300 Ma is suggested from evaporite and BIF occurrences and requires further evaluation.

The correlation between atmospheric oxygenation and supercontinent cycles, has been emphasised by a number of previous studies (Campbell and Squire, 2010; Shield-Zhou and Och, 2011;

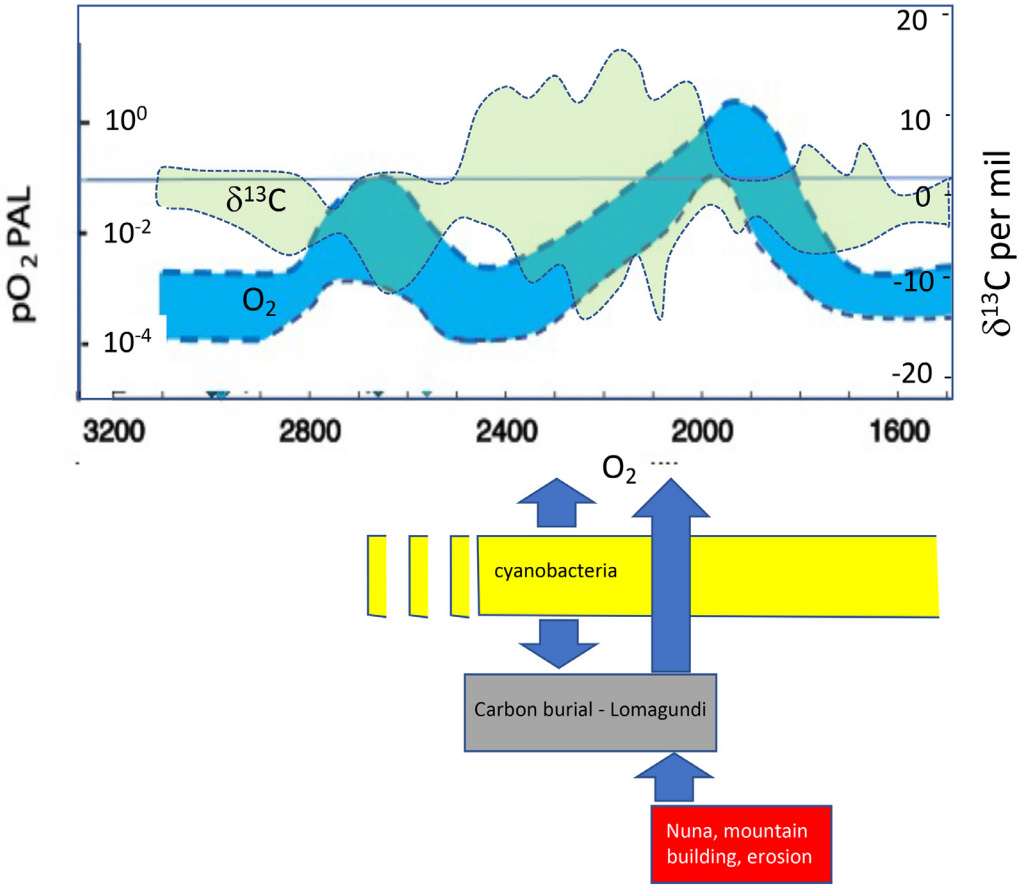

Fig. 7. The preferred scenario for the Paleoproterozoic showing the relationship between predicted atmospheric oxygenation (Fig. 6) and carbon isotope composition of marine carbonates (Fig. 4e). The rise in oxygen levels at the start of the Paleoproterozoic, due to the build-up of cyanobacteria, caused perturbation in the carbon isotope cycle and the burial of organic carbon. This was followed by Earth's second supercontinent cycle, Nuna, that led to the formation of massive mountain ranges whose erosion promoted continuous organic carbon burial extending the Lomagundi event (2400 to 2000 Ma). This led to a renewed and more vigorous oxygen input to the atmosphere that would finally end with the conclusion of Nuna amalgamation and associated active erosion.

Johnson et al., 2017), whereby plate collisions and mountain building represent the orogenic part of the supercontinent cycle, accompanied by active erosion and an increase of nutrient flux to the oceans. This enhanced nutrient flux, in turn, drives productivity, oxygen release, and carbon burial, all of which lead to oxygenation of the atmosphere and oceans. We suggest that stable continents and the subsequent rifting phase of the cycle led to long periods of constant or decreasing atmospheric oxygen as orogenic events became less common and ocean nutrients were gradually drawn down. The coincidence of the orogenic phase of the supercontinent cycles building Kenorland (2800 to 2500 Ma) and Nuna (2100 to 1750 Ma) with our interpreted oxygenation events based on the pyrite proxy, provide important additional support for the proxy. The current position of the GOE, around 2300 Ma, has no obvious relationship to orogenesis or supercontinent cycles, and there is no satisfactory explanation for the relatively sudden rise in atmospheric oxygen at this time.

In contrast our work highlights the possible links between peaks of oxygen production and the Lomagundi event. The data shown in Fig. 7 is consistent with a final Paleoproterozoic oxygen rising due to major organic carbon burial that was probably responsible for the Lomagundi excursion. Thus, the first major rise in oxygen levels at the start of the Paleoproterozoic due to the predominance of cyanobacteria, was followed by Earth's second supercontinental cycle, Nuna, that led to the formation of massive mountain ranges whose erosion promoted continuous organic carbon burial producing the Lomagundi event (2400 to 2000 Ma), leading then to a renewed and more vigorous oxygen input to the atmosphere that would finally end MIF-S and other indicatives of dysoxic/anoxic conditions during the Archean (Fig. 7).

The timing of the first appearance of oxygen-producing cyanobacteria has eluded scientist for many decades now, with interpretations ranging from 3500 to 2200 Ma (Schopf, 2012; Braisier et al., 2002; Shih, 2015). Our multiproxy approach agrees with some researchers, who consider ~2700 Ma as a most likely candidate (Knoll, 2008; Buick, 2008), which supports the premise that there was little if any gap between the evolution of cyanobacteria and the starting point of oxygenation of Earth's atmosphere (Garcia-Pichel et al., 2019). Whether oxygen rose in two main stages between 2700 and 1800 Ma or in several stages is not clear and will require an increased density of sampling and proxy analysis to fill-in the data gaps.

Mineral evolution data clearly document significant changes in Earth's near-surface environment during the Mesoarchean, Neoarchean, and Paleoproterozoic Eras. We observe pulses of mineralization at ~2700 and 2000 Ma, a gradual shift in average mineral redox state, and the introduction of numerous new redox-sensitive mineral species to Earth's near-surface environment. Thus, data on mineral occurrences from the Mesoarchean through the Paleoproterozoic Eras also support the hypothesis of episodic rather than sudden increases in Earth's atmospheric oxygen between 2700 and 1800 Ma.

In conclusion, this analysis throws doubt on the accepted position of the GOE around 2400 to 2200 Ma. We suggest, based on

these multiple independent proxies, that the GOE was not a rapid rise in oxygen over a few tens to one or two hundreds of millions of years, but rather a slow, and pulsed rise over at least 800 million years, which commenced with the first major O_2-producing photosynthesis around 2700 Ma, and continued to rise, eventually peaking at 0.7 to 1 PAL O_2 between 2000 and 1800 Ma.

Author contributions

RRL planned and wrote the first draft, RMH provided data and contributed to the final version, SMM contributed data/figures and contributed to the final version, JAS provided data and contributed to the final version, IM provided data and contributed to the final version and DDG provided data and contributed to the final version.

Declration of Competing Interest

On behalf of the authors I declare no conflict of interest with respect to the enclosed manuscript.

Acknowledgements

We wish to thank the Editors of Geosystems and Geoenvironment for their support in publishing this paper. Also to the extremely helpful and enlightening reviews by Fabricio Caxito and Fernando Tornos.

References

Anbar, A.D., Duan, Y., Lyons, T.W., Arnold, G.L., Kendall, B., Creaser, R.A., Kaufman, A.J., Gordon, G.W., Scott, C., Garvin, J., Buick, R., 2007. A whiff of oxygen before the great oxidation event? Science 317 (5846), 1903–1906.

Brasier, M.D., Green, O.R., Jephcoat, A.P., Kleppe, A.K., Van Kranendonk, M.J., Lindsay, J.F., Steele, A., Grassineau, N.V., 2002. Questioning the evidence for Earth's oldest fossils. Nature 416 (6876), 76–81.

Buick, R., 2008. When did oxygenic photosynthesis evolve? Philos. Trans. R. Soc. Lond. B. Biol. Sci. 363 (1504), 2731–2743.

Campbell, I.H., Squire, R.J., 2010. The mountains that triggered the late neoproterozoic increase in oxygen: the second great oxidation event. Geochim. Cosmochim. Acta 74, 4187.

Catling, D.C., Kasting, J.F., 2017. Atmospheric Evolution On Inhabited and Lifeless Worlds. Cambridge University Press.

Cloud, P., 1972. A working model of the primitive earth. Am. J. Sci. 272 (6), 537–548.

Cheng, C., Busigny, V., Ader, M., Thomazo, C., Chaduteau, C., Philippot, P., 2019. Nitrogen isotope evidence for stepwise oxygenation of the ocean during the great oxidation event. Geochim. Cosmochim. Acta 261, 224–247.

Cole, D.B., Reinhard, C.T., Wang, X., Gueguen, B., Halverson, G.P., Gibson, T., Hodgskiss, M.S., McKenzie, N.R., Lyons, T.W., Planavsky, N.J., 2016. A shale-hosted Cr isotope record of low atmospheric oxygen during the Proterozoic. Geology 44 (7), 555–558.

Condie, K.C., Des Marais, D.J., Abbott, D., 2001. Precambrian superplumes and supercontinents: a record in black shales, carbon isotopes, and paleoclimates? Precambrian Res 106 (3–4), 239–260.

Evans, D.A., 2006. Proterozoic low orbital obliquity and axial-dipolar geomagnetic field from evaporite palaeolatitudes. Nature 444 (7115), 51–55.

Farquhar, J., Wing, B.A., 2003. Multiple sulfur isotopes and the evolution of the atmosphere. EPSL 213, 1–13.

Farquhar, J., Bao, T., Thiemens, M., 2000. Atmospheric influence of earth's earliest sulfur cycle. Science 289, 756–759.

Farquhar, J., Zerkle, A.L., Bekker, A., 2011. Geological constraints on the origin of oxygenic photosynthesis. Photosyn. Res. 107 (1), 11–36.

Fang, Z., Qin, L., Liu, W., Yao, T., Chen, X., Wei, S., 2020. Absence of hexavalent chromium in marine carbonates: implications for chromium isotopes as paleoenvironment proxy. Natl. Sci. Rev. 8 (3) nwaa090.

Frei, R., Gaucher, C., Poulton, S.W., Canfield, D.E., 2009. Fluctuations in precambrian atmospheric oxygenation recorded by chromium isotopes. Nature 461 (7261), 250–253.

Garcia-Pichel, F., Lombard, J., Soule, T., Dunaj, S., Wu, S.H., Wojciechowski, M.F., 2019. Timing the evolutionary advent of cyanobacteria and the later great oxidation event using gene phylogenies of a sunscreen. MBio 10 (3) e00561-19.

Golden, J.J., 2019. Mineral Evolution Database: Data Model For Mineral Age Associations. Masters Thesis, Univ. of Arizona, Tucson, AZ.

Golden, J.J., McMillan, M., Downs, R.T., Hystad, G., Goldstein, H.J., Zimmerman, A., Sverjensky, D.A., Armstrong, J.T., Hazen, R.M., 2013. Rhenium variations in molybdenite (MoS2): evidence for progressive subsurface oxidation. Earth Planet. Sci. Lett. 366, 1–5.

Hazen, R.M., Papineau, D., Bleeker, W., Downs, R.T., Ferry, J.M., McCoy, T.J., Sverjensky, D.A., Yang, H., 2008. Mineral evolution. Am. Mineral. 93 (11–12), 1693–1720.

Holland, H.D., 1984. The Chemical Evolution of the Atmosphere and Oceans. Princeton University Press, Princeton.

Hummer, D.R., Hystad, G., Golden, J.J., Liu, C., Downs, R.T., Morrison, S.M., Grew, E.S., Hazen, R.M., 2020. Manganese mineral ecology. Am. Mineral. in press.

Johnson, S.C., Large, R.R., Coveney, R.M., Kelley, K.D., Slack, J.F., Steadman, J.A., Gregory, D.D., Sack, P.J, Meffre, S., 2017. Secular distribution of highly metalliferous black shales corresponds with peaks in past atmosphere oxygenation. Min. Dep. 52 (6), 791–798.

Killingsworth, B.A., Sansjofre, P., Philippot, P., Cartigny, P., Thomazo, C., Lalonde, S.V., 2019. Constraining the rise of oxygen with oxygen isotopes. Nat. Commun. 10, 4929. doi:10.1038/s41467-019-12883-2.

Kappler, A., Pasquero, C., Konhauser, K.O., Newman, D.K., 2005. Deposition of banded iron formations by anoxygenic phototrophic Fe (II)-oxidizing bacteria. Geology 33 (11), 865–868.

Knoll, A.H., 2008. Cyanobacteria and earth history. The Cyanobacteria: Mol. Biol. Evol. 484.

Lalonde, S.V., Konhauser, K.O., 2015. Benthic perspective on Earth's oldest evidence for oxygenic photosynthesis. P. Natl. Acad. Sci. USA. 112 (4), 995–1000.

Large, R.R., Mukherjee, I., Zhukova, I., Corkrey, R., Stepanov, A., Danyushevsky, L.V., 2018. Role of upper-most crustal composition in the evolution of the precambrian ocean-atmosphere system. Earth Planet. Sci. Lett. 487, 44–53.

Large, R.R., Halpin, J.A., Danyushevsky, L.V., Maslennikov, V.V., Bull, S.W., Long, J.A., Gregory, D.D., Lounejeva, E., Lyons, T.W., Sack, P.J., McGoldrick, P.J., 2014. Trace element content of sedimentary pyrite as a new proxy for deep-time ocean–atmosphere evolution. Earth Panet. Sci. Lett. 389, 209–220.

Large, R.R., Mukherjee, I., Gregory, D.D., Steadman, J.A., Maslennikov, V.V., Meffre, S., 2017. Ocean and atmosphere geochemical proxies derived from trace elements in marine pyrite: implications for ore genesis in sedimentary basins. Econ. Geol. 112 (2), 423–450.

Lyons, T., Reinhard, C.T., Planavsky, N.J., 2014. The rise of oxygen in earth's early ocean and atmosphere. Nature 506, 307–315.

Meixnerová, J., Blum, J.D., Johnson, M.W., Stüeken, E.E., Kipp, M.A., Anbar, A.D., Buick, R., 2021. Mercury abundance and isotopic composition indicate subaerial volcanism prior to the end-Archean "whiff" of oxygen. P. Natl. Acad. Sci. USA. 118 (33).

Melezhik, V.A., Huhma, H., Condon, D.J., Fallick, A.E., Whitehouse, M.J., 2007. Temporal constraints on the Paleoproterozoic Lomagundi-Jatuli carbon isotopic event. Geology 35 (7), 655–658.

Mukherjee, I., Large, R.R., 2016. Pyrite trace element chemistry of the Velkerri Formation, Roper Group, McArthur Basin: evidence for atmospheric oxygenation during the boring billion. Precambrian Res 281, 13–26.

Ohmoto, H., Watanabe, Y., Ikemi, H., Poulson, S.R., Taylor, B.E., 2006. Sulphur isotope evidence for anoxic Archaean atmosphere. Nature 442 (7105), 908–911.

Ostrander, C.M., Johnson, A.C., Anbar, A.D., 2021. Earth's first redox revolution. Annu. Rev. Earth Planet Sci. 49, 337–366.

Ossa, F.O., Hofmann, A., Spangenberg, J.E., Poulton, S.W., Stüeken, E.E., Schoenberg, R., Eickmann, B., Wille, M., Butler, M., Bekker, A., 2019. Limited oxygen production in the Mesoarchean ocean. P. Natl. Acad. Sci. USA. 116 (14), 6647–6652.

Pavlov, A.A., Kasting, J.F., 2002. Mass-independent fractionation of sulfur isotopes in Archean sediments: strong evidence for an anoxic Archean atmosphere. Astrobiology 2 (1), 27–41.

Payne, J.L., Boyer, A.G., Brown, J.H., Finnegan, S., Kowalewski, M., Krause, R.A., Lyons, S.K., McClain, C.R., McShea, D.W., Novack-Gottshall, P.M., Smith, F.A., 2009. Two-phase increase in the maximum size of life over 3.5 billion years reflects biological innovation and environmental opportunity. P. Natl. Acad. Sci. USA. 106 (1), 24–27.

Philippot, P., Ávila, J.N., Killingsworth, B.A., Tessalina, S., Baton, F., Caquineau, T., Muller, E., Pecoits, E., Cartigny, P., Lalonde, S.V., Ireland, T.R., 2018. Globally asynchronous sulphur isotope signals require re-definition of the great oxidation event. Nat. Commun. 9 (1), 1–10.

Planavsky, N.J., Reinhard, C.T., Wang, X., Thomson, D., McGoldrick, P., Rainbird, R.H., Johnson, T., Fischer, W.W., Lyons, T.W., 2014. Low mid-proterozoic atmospheric oxygen levels and the delayed rise of animals. Science 346 (6209), 635–638.

Planavsky, N.J., Robbins, L.J., Kamber, B.S., Schoenberg, R., 2020. Weathering, alteration and reconstructing earth's oxygenation. Interface Focus 10 (4), 20190140.

Schopf, J.W., 2012. The fossil record of cyanobacteria. In: Ecology of Cyanobacteria II. Springer, Dordrecht, pp. 15–36.

Scott, C., Lyons, T.W., Bekker, A., Shen, Y., Poulton, S.W., Chu, X., Anbar, A.D., 2008. Tracing the stepwise oxygenation of the proterozoic ocean. Nature 452, 456–459.

Shields, G., Veizer, J., 2002. Precambrian marine carbonate isotope database: version 1.1. Geochem. Geophys. Geosyst. 3 (6), 1–12.

Shields-Zhou, G., Och, L., 2011. The case for a neoproterozoic oxygenation event: geochemical evidence and biological consequences. GSA Today 21 (3), 4–11.

Shih, P.M., 2015. Cyanobacterial evolution: fresh insight into ancient questions. Curr. Biol. 25 (5), R192–R193.

Steadman, J.A., Large, R.R., Blamey, N.J., Mukherjee, I., Corkrey, R., Danyushevsky, L.V., Maslennikov, V., Hollings, P., Garven, G., Brand, U., Lécuyer, C., 2020. Evidence for elevated and variable atmospheric oxygen in the precambrian. Precambrian Res, 105722.

Stüeken, E.E., Kipp, M.A., Koehler, M.C., Buick, R., 2016. The evolution of earth's biogeochemical nitrogen cycle. Earth Sci. Rev. 160, 220–239.

Thoby, M., Konhauser, K.O., Fralick, P.W., Altermann, W., Visscher, P.T., Lalonde, S.V.,

2019. Global importance of oxic molybdenum sinks prior to 2.6 Ga revealed by the Mo isotope composition of precambrian carbonates. Geology 47 (6), 559–562.
Towe, K.M., 1990. Aerobic respiration in the Archean? Nature 348 (6296), 54–56.
Wille, M., Kramers, J.D., Nägler, T.F., Beukes, N.J., Schröder, S., Meisel, T., Lacassie, J.P., Voegelin, A.R., 2007. Evidence for a gradual rise of oxygen between 2.6 and 2.5 Ga from Mo isotopes and *Re*-PGE signatures in shales. Geochim. Cosmochim. Acta 71 (10), 2417–2435.